

Article

A Comparison of Optimal Operation of a Residential Fuel Cell Co-Generation System Using Clustered Demand Patterns Based on Kullback-Leibler Divergence

Akira Yoshida ^{1,*}, Yoshiharu Amano ¹, Noboru Murata ², Koichi Ito ¹ and Takumi Hasizume ¹

¹ Research Institute for Science and Engineering, Waseda University, 17 Kikui-cho, Shinjuku-ku, 162-0044, Tokyo, Japan; E-Mails: yoshiha@waseda.jp (Y.A.); koichi-ito@waseda.jp (K.I.); hasizume@waseda.jp (T.H.)

² School of Science and Engineering, Waseda University, 1-4-3 Okubo, Shinjuku-ku, 169-8555, Tokyo, Japan; E-Mail: noboru.murata@eb.waseda.ac.jp

* Author to whom correspondence should be addressed; E-Mail: yoshida@power.mech.waseda.ac.jp; Tel.: +81-3-3203-4437; Fax: +81-3-3203-3231.

Received: 9 November 2012; in revised form: 3 December 2012 / Accepted: 21 December 2012 /

Published: 16 January 2013

Abstract: When evaluating residential energy systems like co-generation systems, hot water and electricity demand profiles are critical. In this paper, the authors aim to extract basic time-series demand patterns from two kinds of measured demand (electricity and domestic hot water), and also aim to reveal effective demand patterns for primary energy saving. Time-series demand data are categorized with a hierarchical clustering method using a statistical pseudo-distance, which is represented by the generalized Kullback-Leibler divergence of two Gaussian mixture distributions. The classified demand patterns are built using hierarchical clustering and then a comparison is made between the optimal operation of a polymer electrolyte membrane fuel cell co-generation system and the operation of a reference system (a conventional combination of a condensing gas boiler and electricity purchased from the grid) using the appropriately built demand profiles. Our results show that basic demand patterns are extracted by the proposed method, and the heat-to-power ratio of demand, the amount of daily demand, and demand patterns affect the primary energy saving of the co-generation system.

Keywords: co-generation; demand pattern; Gaussian mixture model; hierarchical clustering; KL-divergence; optimal operation

Nomenclature:

c	specific heat of water
C	conversion factor
D	distance measure
\mathcal{D}	distance matrix
e, E	electricity
f, f'	a probability density function
\tilde{f}, \tilde{f}'	Gaussian probability density function
g, G	gas consumption
H	heating value
J	primary energy consumption, MJ/day
k	discretized index
K	number of discrete value
$p, \tilde{p}, p', \tilde{p}'$	Gaussian mixture distribution
q	amount of heat
Q	DHW demand
R	heat-to-power ratio
t	discretized time index
T	number of time index
\mathbf{x}	vector of continuous variables
V	tank capacity
\mathbf{z}	vector of binary variables

Greek Symbols

α	slope
β	intercept
γ	contribution ratio, %
δt	sampling period, hour
η	efficiency, %
θ	temperature, °C
λ	unknown parameters
μ	mean vector
π	mixing coefficient
ρ	water density
Σ	covariance matrix
φ	primary energy reduction ratio, %

Subscripts and Superscripts

a, b	component index of the Gaussian mixture distribution
AUXS	auxiliary
B	boiler
buy	buying
C	controller
day	daytime
dem	demand
ELE	non-HVAC electricity demand
e	electricity
$\tilde{f}, \tilde{f}', p, p'$	a probability density function
P1, P2, P3	pump
FC	fuel cell
g	Gaussian distribution
gas	gas
gen	generalized
gm	Gaussian mixture distribution
H	electric heater
HW	hot water demand
HWT	thermal storage tank
i	start-up term
in	inlet
KL	KL divergence
night	nighttime
out	outlet
q	thermal
rate1, rate2	piecewise-linear term
R	radiator fan
RS	reference system
symm	symmetrized
up	start-up
W	water
X	each device

1. Introduction

A variety of water heaters are commercially available in Japan. Condensing gas boilers and heat pump water heaters, which operate with CO₂ as a working fluid, and co-generation systems (CGS), which have polymer electrolyte fuel cells, are available. Residential energy consumption has been increasing slowly but surely in Japan [1], and accounted for 63.3% of all residential energy consumption from domestic hot water (DHW) and electricity (excluding heating, ventilation and air conditioning (HVAC)) demands in 2001 [2]. Energy consumption in Japan for cooling accounts for only 2.4% of annual demand per household [2]. On the other hand, energy consumption for heating accounts for 29.3% of annual demand [2]. Residential energy demand varies widely in terms of time-series behaviors, amounts consumed between households, and even within one household. Residential energy demand profiles have a high degree of uncertainty in their essentials because of the occupant-driven load. When evaluating residential energy systems, demand profiles are critical. In order to reduce the primary energy consumption when introducing an energy supply system, we need rational energy system selection guidelines and rational operation strategies that consider a variety of demand profiles. Hence, it is important to clarify the matches between the characteristics of energy systems and the characteristics of demand profiles.

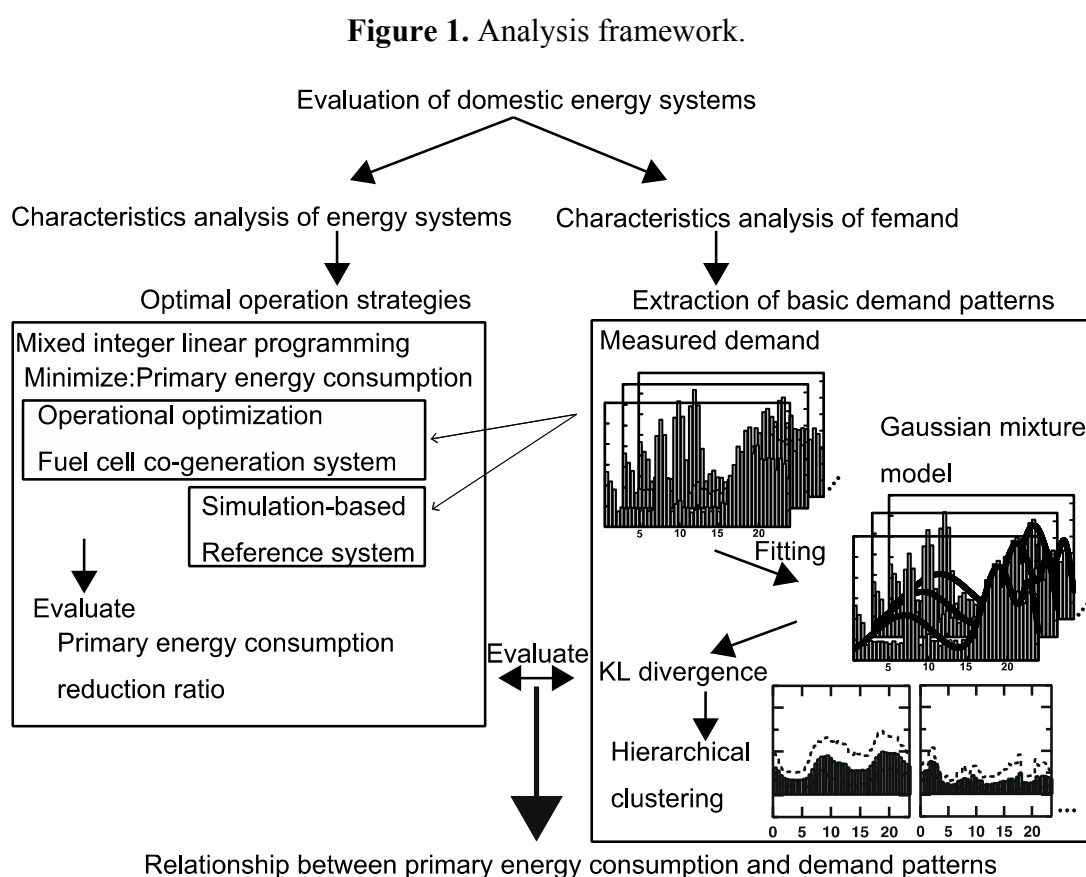
Co-generation systems with energy buffers have a lot of operational flexibility, therefore, it is difficult to judge the best operation for the energy saving. Mathematical programming is useful to know their optimal operation strategies for the energy saving. The optimal operational planning for a gas engine co-generation system with thermal storage was proposed by many researchers, such as Yokoyama *et al.* [3] using a Mixed Integer Linear Programming (MILP) method. Wakui *et al.* [4] compared optimal operations of heat-led and power-led using this method for a solid oxide fuel cell co-generation system. Basically, this study adapts those frameworks for leading optimal operations of a co-generation system. Hashimoto *et al.* [5] carried out a comparative evaluation on both a CO₂ heat-pump system and two kinds of polymer electrolyte membrane fuel cell co-generation systems (PEFC-CGS). At that time, because there were no commercial PEFC-CGSs, they estimated the model parameters with assumptions based on an ideal physics model, and these systems operated on the basis of twelve demand patterns of monthly representative days, unlike our study using the data of an available CGS. A number of researchers have addressed the problems, which are represented with mathematical models of co-generation systems using a lot of measured demand data; for example, an early study developed simulation models of residential-scale co-generation from prototypes, and revealed their energy saving potential in Annex 42 of the International Energy Agency [6]. In another early study, the above methodology framework was applied to an evaluation of condensing gas boiler and heat pump technologies with various loads [7].

In our previous study [8], the daily optimal operations of the PEFC-CGS and the CO₂ heat-pump system were analyzed using data from systems in operation and from measured demand. It showed that primary energy consumption is reduced when an energy system is introduced with characteristics matching the characteristics of the demand profiles. Thus, one of the selection criteria when introducing an energy system is the amount and the heat-to-power ratio of daily demand. The primary energy consumption of the PEFC-CGS shows large differences in spite of the similarity in the amount of daily demand and the similarity of the heat-to-power ratio of non-HVAC electricity and DHW

demand. We guess that other factors affect the primary energy consumption of each system. Here we hypothesize that demand patterns have an effect on the primary energy consumption. We can not find the study, which reveal the effect of time-series demand patterns for the operation of the CGSs, therefore, make an analysis of the demand patterns. In this paper, main objectives are:

1. To extract basic time-series demand patterns from the data of a system in operation and 26307 days of data for two kinds of demand (non-HVAC electricity and DHW), and
2. To reveal effective demand patterns for the primary energy reduction of the PEFC-CGS.

Figure 1 shows the analysis framework of this paper.



Demand time-series data are categorized by means of a kind of "unsupervised" learning [9], which is a hierarchical clustering method using a statistical pseudo-distance. The statistical pseudo-distance is represented by the generalized Kullback-Leibler (KL) divergence [10] of two Gaussian Mixture Distributions (GMDs) fitted to the time-series demand data. The unsupervised learning method for electricity consumption was proposed by Shen *et al.* [11]; This paper extend the scope of its application not only for electricity but also for a combination of electricity and DHW demand in order to evaluate the co-generation system. A previous report [12] did clustering analysis directly using the energy consumption data, unlike our approach using model-based clustering. Clustering analysis, which is listed in detail, has been reported by Liao [13]. Our classified clusters are evaluated by the optimal operation of the PEFC-CGS. The main consideration is the relationship between the clustered time-series demand data and the primary energy consumption of one PEFC-CGS. The PEFC-CGS is compared to a reference system (R-S): a combination of a condensing gas boiler and electricity

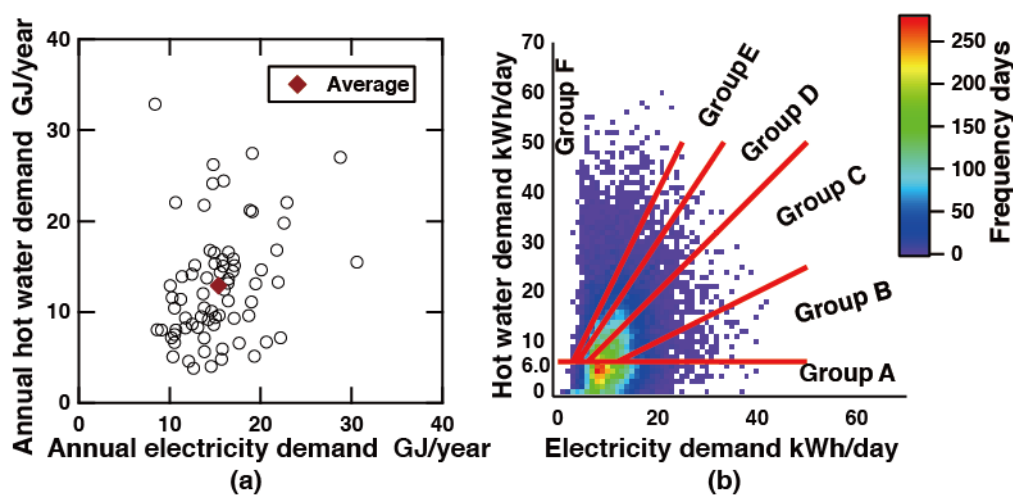
purchased from the grid, because the PEFC-CGS competes with the R-S when installing appliances for a new house.

This paper evaluates the energy saving potential of the PEFC-CGS, by using model of a state-of-art, available performance data, and the relationship with demand patterns using clustering techniques on a combination of electricity and DHW demand.

2. Hot Water and Non-HVAC Electricity Demand

Figure 2 shows demand maps measured in 40 households in detached houses and 32 households in residential apartment buildings. The energy consumption data is for a total of 26,307 days, which include days of leap years, and were measured by Tsuji *et al.* [14] in Kinki region around Osaka with a sampling interval of 30 minutes. The data was decomposed to specified usages. The usages represent electricity and gas consumption, for space cooling, space heating, cooking, hot water, and other, respectively [14]. Those were multiplied the equipment efficiencies by applications, and were reclassified to five different kinds of demand: space cooling, space heating, cooking, DHW, and non-HVAC electricity. The numbers of occupants are between three and six. The Kinki region is located near the left-of-center of the main island in Japan, therefore, it seems to represent average houses in Japan. As shown in Figure 2a, the annual non-HVAC electricity demand is 15.49 GJ/year (about 11.79 kWh/day), and the annual DHW demand is 13.05 GJ/year (about 9.93 kWh/day), on average, for the 72 households.

Figure 2. Measured demand. (a) annual; (b) daily.



As shown in Figure 2(b), the modal value of the daily non-HVAC electricity demand, E , is around 8 kWh/day, and the modal value of daily DHW demand, Q , is around 4 kWh/day. Daily demand varies widely with DHW demand reaching over 60 kWh/day in some cases, which is 15 times the modal value. The PEFC-CGS, which is discussed later in Section 4, has a thermal storage tank, which has about 10 kWh capacity. Thermal-load leveling by the thermal storage tank seems to have the effect for only few days at the most, because daily averaged DHW demand is the same level of the capacity of the thermal storage tank. Since the operational strategy might be implemented in co-generation systems on a daily time scale, time-series data should be analyzed on the same scale. In order to reveal

the energy saving potential of the solely PEFC-CGS, this paper targets non-HVAC electricity and DHW demand, and uses only time-series demand data of all 72 households for the extraction of demand patterns. Demographic data is not used so that it could be focus on the effect of demand patterns. When revealing the energy saving potential in each household, this paper represents a method to evaluate the collection of one-day demand patterns as the characteristics of a household.

As shown in Figure 2(b), measured demand data are separated from the daily heat-to-power ratio, R , and DHW demand, Q , by red lines. For descriptive purposes as shown in Table 1, the 26,307 days are divided into six sets of groups, defined by each zone of heat-to-power ratio, R . The measured demand data are separated based on information obtained from our earlier study [8]: the fuel cell unit is inefficient when underused; the PEFC-CGS increases primary energy consumption compared with the R-S in the zone under $Q = 6$ kWh/day. We do a clustering analysis for each group.

Table 1. Demand groups.

Group name	Number of elements, days	DHW demand Q , kWh/day	Heat-to-power ratio R
A	9807	$Q < 6.0$	---
B	971	$6.0 \leq Q$	$R < 0.5$
C	6958	$6.0 \leq Q$	$0.5 \leq R < 1.0$
D	4920	$6.0 \leq Q$	$1.0 \leq R < 1.5$
E	1926	$6.0 \leq Q$	$1.5 \leq R < 2.0$
F	1725	$6.0 \leq Q$	$2.0 \leq R < \infty$

3. Clustering Model

Time-series demand data are categorized by a hierarchical clustering method using a statistical pseudo-distance. A statistical pseudo-distance is the distance between two points in a pseudo-metric, which is defined by the identity of indiscernibles, symmetry and triangle inequality. The statistical pseudo-distance is calculated from the generalized KL divergence with the GMD fitted to the time-series demand data. Actually, this process fits the GMD to some peaks of the daily non-HVAC electricity and DHW demands. The GMD is represented by three parameters: the mean, the covariance, and the coefficient in the linear combination. 48-dimensional vectors, which are 48 terms accumulated every 30 minutes through a day, are translated to vectors with up to 12 dimensions. The time-series demand data are categorized by the hierarchical clustering method using the distance, which is calculated with information per day represented by vectors with up to 12 dimensions. The KL divergence, which represents the dissimilarity measure between two distributions, is often used for cluster analyses. The Bregman divergence [15] is a pseudo-distance for measuring the discrepancy between two functions. The generalized KL divergence is extended by the framework of the Bregman divergence, and can handle distributions and others. In this paper, the generalized KL divergence between two biased distributions, which represents the dissimilarity measure of the histogram of daily time-series demand data, is used as the pseudo-distance of the clustering. Readers are referred to Shen *et al.* [11] for details.

3.1. Gaussian Mixture Model

For a T -dimensional vector $\mathbf{x} = (x_1, \dots, x_T)^\top$ of continuous variables, the Gaussian distribution (GD) is defined by

$$\mathcal{N}(\mathbf{x}|\boldsymbol{\mu}, \boldsymbol{\Sigma}) = \frac{1}{(2\pi)^{\frac{T}{2}}} \frac{1}{|\boldsymbol{\Sigma}|^{\frac{1}{2}}} \exp\left\{-\frac{1}{2}(\mathbf{x} - \boldsymbol{\mu})^\top \boldsymbol{\Sigma}^{-1}(\mathbf{x} - \boldsymbol{\mu})\right\} \quad (1)$$

where $\boldsymbol{\mu}$ is a T -dimensional mean vector, and $\boldsymbol{\Sigma}$ is a $T \times T$ covariance matrix. A superposition of K Gaussian densities of the form:

$$p(\mathbf{x}|\boldsymbol{\lambda}) = \sum_{k=1}^K \pi_k \mathcal{N}(\mathbf{x}|\boldsymbol{\mu}_k, \boldsymbol{\Sigma}_k) \quad (2)$$

is called a mixture of Gaussians. The π parameters are called mixing coefficients. If we integrate both sides of Equation (2) with respect to \mathbf{x} , and note that both $p(\mathbf{x})$ and the individual Gaussian components are normalized, we obtain:

$$\sum_{k=1}^K \pi_k = 1 \quad (3)$$

The form of the GMD is governed by the parameters $\boldsymbol{\pi} \equiv \{\pi_1, \dots, \pi_K\}$, $\boldsymbol{\mu} \equiv \{\boldsymbol{\mu}_1, \dots, \boldsymbol{\mu}_K\}$, $\boldsymbol{\Sigma} \equiv \{\boldsymbol{\Sigma}_1, \dots, \boldsymbol{\Sigma}_K\}$. Here, the unknown parameters $\boldsymbol{\lambda}$ are defined by:

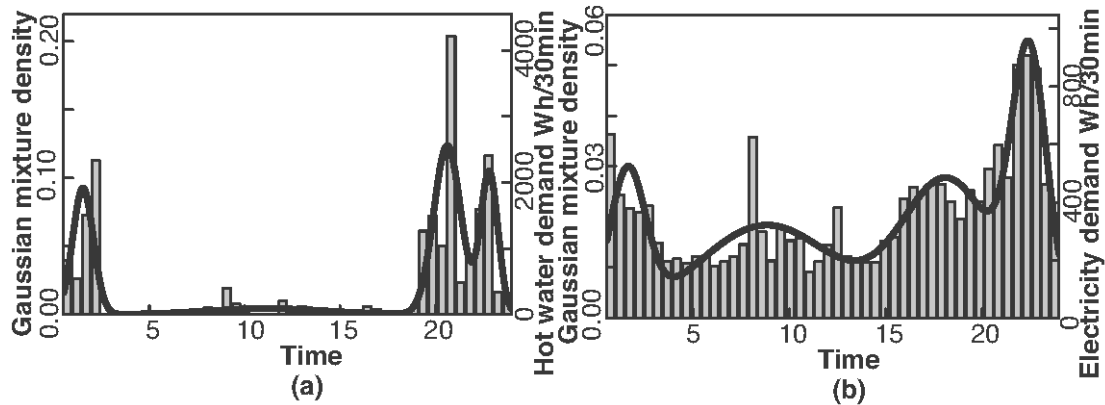
$$\boldsymbol{\lambda} = \{\pi_k, \boldsymbol{\mu}_k, \boldsymbol{\Sigma}_k\}_{k=1}^K \quad (4)$$

The unknown parameters $\boldsymbol{\lambda}$ in the GMD are determined by maximizing the likelihood function. The maximum likelihood solution for the parameters does not have a closed-form analytical solution. Using the Expectation-Maximization (EM) algorithm [16], to estimate the parameters of the Gaussian mixture model. The EM algorithm is a method of approximating inference.

We utilized the Mclust function [17] with mclust packages in R language, which is an open source programming language and software environment for statistical computing. The numbers of the Gaussian mixture elements are chosen by the Bayesian Information Criterion (BIC) [18] from one to four. In other words, the GMD fits the demand patterns, which might have up to four peaks in a day, at morning, noon, evening and midnight. In this process, 48-dimensional daily demand vectors are represented by a maximum of $3 \times 4 = 12$ -dimensional vectors of the GMD, because the GMD is represented the three parameters, namely the mean, the covariance, and the coefficient in the linear combination.

Figure 3 shows a sample fitting of the Gaussian mixture model for time-series demand data. In Figure 3(a), the bar charts represent the hot water demand of a sample day, and the solid curves represent the Gaussian mixture density. There are three major peaks and one minor peak, corresponding to the four GDs. Similarly, as shown in Figure 3(b), the non-HVAC electricity demand of this sample day has four peaks.

Figure 3. A sample fitting of the Gaussian mixture model. (a) Hot water demand; (b) electricity demand.



3.2. Kullback-Leibler Divergence

Statistical pseudo-distances between all days are represented by the KL divergence, which is known as the “relative entropy”. The KL divergence between two probability density functions, $f(x)$ and $f'(x)$, is given by:

$$D_{KL}(f, f') = \int f(x) \ln \frac{f(x)}{f'(x)} dx \tag{5}$$

The KL divergence between T -dimensional GDs $\tilde{f}(x)$ and $\tilde{f}'(x)$ is given by:

$$D_g(\tilde{f}, \tilde{f}') = \frac{1}{2} \left[\log \frac{|\Sigma_{\tilde{f}'}|}{|\Sigma_{\tilde{f}}|} + \text{Tr} \left[\Sigma_{\tilde{f}'}^{-1} \Sigma_{\tilde{f}} \right] - T + (\mu_{\tilde{f}} - \mu_{\tilde{f}'})^T \Sigma_{\tilde{f}'}^{-1} (\mu_{\tilde{f}} - \mu_{\tilde{f}'}) \right] \tag{6}$$

The KL divergence between two mixtures of Gaussian $p(x|\lambda)$ and $p'(x|\check{\lambda})$ is approximated by:

$$D_{gm}(p, p') = \sum_{a=1}^{K_a} \pi_a \log \frac{\sum_{\check{a}=1}^{K_{\check{a}}} \pi_{\check{a}} \exp \left(-D_g(p_a, p_{\check{a}}) \right)}{\sum_{b=1}^{K_b} \pi_b \exp \left(-D_g(p_a, p'_b) \right)} \tag{7}$$

where Gaussian, $p_a(x)$, is the a^{th} component of the GMD $p(x|\lambda)$. Specifically, in this context, x represents the measured demand of a day, $p(x|\lambda)$ represents the characteristics of one day of the waveform regarding time-series demand data as a histogram, and $p_a(x)$ represents the characteristics of a peak fitted to the GD. $p'(x)$ represents the characteristic of the wave form of the other day. Up to this point, we have considered the KL divergence as the difference between the shapes of the histograms of the daily time-series demand data. In this paper, it is important to consider both the daily total demand and the time-series behaviors, because the balance of electricity and heat demand is critical for CGS performance. Here, we consider a biased GMD, $\tilde{p}(x)$ for one day and $\tilde{p}'(x)$ for the other day, which are multiplied by the daily total non-HVAC electricity demand, $E_p, E_{p'}$, kWh/day. The KL divergence of non-HVAC electricity demand is explained in the following context:

$$\tilde{p}(x) = \frac{E_p}{1000} p(x) \tag{8}$$

$$\tilde{p}'(x) = \frac{E_{p'}}{1000} p'(x) \tag{9}$$

For calculating the KL divergence from the biased GMD, (8), the generalized KL divergence, \mathcal{D}_{gen} , which is extended by the framework of the Bregman divergence, is given by:

$$\begin{aligned} \mathcal{D}_{\text{gen}}(\tilde{p}, \tilde{p}') &= \int_x \left(\tilde{p}(x) \log \frac{\tilde{p}(x)}{\tilde{p}'(x)} - \tilde{p}(x) + \tilde{p}'(x) \right) dx \\ &= \frac{E_p}{1000} \mathcal{D}_{\text{gm}}(p, p') + \frac{E_p}{1000} \log \frac{E_p}{E_{p'}} - \frac{E_p}{1000} + \frac{E_{p'}}{1000} \end{aligned} \tag{10}$$

The KL divergence is not a symmetrical quantity, that is to say $\mathcal{D}_{\text{gen}}(\tilde{p}, \tilde{p}') \neq \mathcal{D}_{\text{gen}}(\tilde{p}', \tilde{p})$. In order to use the KL divergence for a distance measure in cluster analysis, we adopt the symmetrized KL divergence, $\mathcal{D}_{\text{symm}}^{\text{ELE}}$, given by:

$$\mathcal{D}_{\text{symm}}^{\text{ELE}}(\tilde{p}, \tilde{p}') = \frac{\mathcal{D}_{\text{gen}}(\tilde{p}, \tilde{p}') + \mathcal{D}_{\text{gen}}(\tilde{p}', \tilde{p})}{2} \tag{11}$$

The distance matrix, $\mathcal{D}_{\text{symm}}^{\text{ELE}}$, for the clustering is composed of the symmetrized KL divergences. The symmetrized KL divergence for DHW demand $\mathcal{D}_{\text{symm}}^{\text{HW}}$, and the distance matrix $\mathcal{D}_{\text{symm}}^{\text{HW}}$ are also calculated in the same manner.

3.3. Hierarchical Clustering

The hierarchical clustering analysis uses a distance matrix, \mathcal{D} , with the KL divergence of both non-HVAC electricity and DHW demands as the distance measure between clusters from Ward’s method [19]. Because both distance matrices, $\mathcal{D}_{\text{symm}}^{\text{ELE}}$ and $\mathcal{D}_{\text{symm}}^{\text{HW}}$, are calculated independently to this point, they are normalized by dividing by the median of each $\mathcal{D}_{\text{symm}}^{\text{ELE}}$ and $\mathcal{D}_{\text{symm}}^{\text{HW}}$ in order to compute the sum of the two distance matrices. The distance matrix, \mathcal{D} , which sums the two kinds of symmetrized KL divergence, is given by:

$$\mathcal{D} = \frac{\mathcal{D}_{\text{symm}}^{\text{ELE}}}{\text{Median}(\mathcal{D}_{\text{symm}}^{\text{ELE}})} + \frac{\mathcal{D}_{\text{symm}}^{\text{HW}}}{\text{Median}(\mathcal{D}_{\text{symm}}^{\text{HW}})} \tag{12}$$

where “Median” represents the median of the matrix. Demand is classified into 16 clusters for each group using the hierarchical clustering method. The reason for 16 clusters is because we assume DHW demand patterns vary widely while non-HVAC electricity demand patterns do not. In other words, $2^4 = 16$ clusters represent the combination of the four existing or non-existing DHW demand peaks, which are morning, noon, evening and midnight.

4. Polymer Electrolyte Membrane Fuel Cell Co-Generation System Model

The clusters, which are classified in the previous section, are evaluated relative to the optimal operation of the PEFC-CGS. Again, the main consideration is the relationship between the clustered time-series demand data and the primary energy consumption of the PEFC-CGS. The PEFC-CGS is compared to the R-S. Schematic diagrams with the specifications [8] of the PEFC-CGS, and the R-S are shown below. The parameters in the model are taken from public information [20]. This problem is formulated as a MILP problem. The models were coded by the algebraic modeling language AMPL version 12.1 [21] as the conventional MILP, and were solved by the general optimization solver CPLEX version 12.1 [22].

4.1. Objective Function

The objective function to be minimized is the daily primary energy consumption calculated from the summation of purchased electricity, e^{buy} , and gas consumption, g^{buy} , multiplied by each primary energy conversion factor. In particular, the primary energy consumption of purchased gas is converted using the higher heating value of C^{gas} , 45 MJ/m³ [23]. The primary energy conversion factors of electricity mean all of the conversion efficiencies from power plants to end users. In other words, they include transmission losses, the efficiency of power plants and so on. The primary energy conversion factor of purchased electricity in the daytime is C_{day}^e , 9.97 MJ/kWh [24], and the primary energy conversion factor of purchased electricity in the nighttime is C_{night}^e , 9.28 MJ/kWh [24]. The objective function J , which is the daily operating cost from the viewpoint of the primary energy consumption, is given by:

$$J = \sum_{t=1}^T \left(C_{\text{day}}^e e_{\text{day}}^{\text{buy}}(t) + C_{\text{night}}^e e_{\text{night}}^{\text{buy}}(t) + C^{\text{gas}} g^{\text{buy}}(t) \right) \quad (13)$$

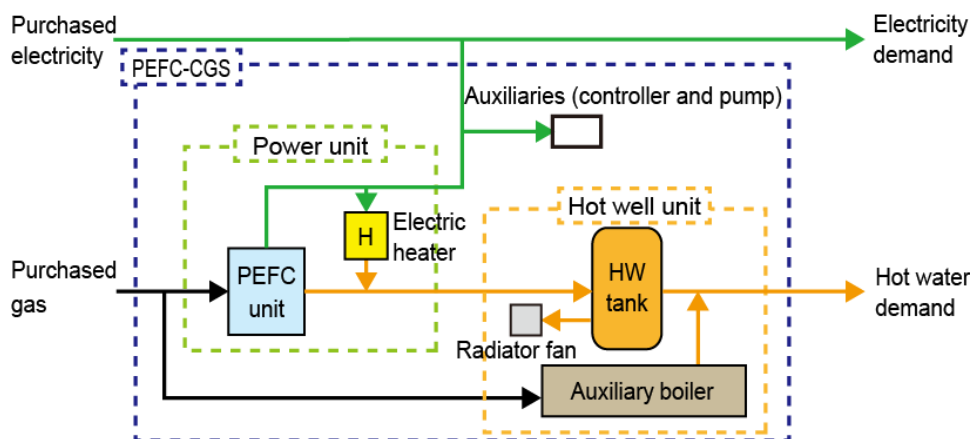
where $t = 1, \dots, T$ represents the time index. T is the number of time periods. The sampling period, δt , is 0.5 hours. One day is discretized to $T = 48$ terms. We stack the optimal solutions and operations for each day to evaluate the characteristics of the PEFC-CGS.

4.2. Constraints

The X kinds of T -dimensional continuous non-negative decision variables vectors, electricity consumption $e^X = (e^X(1), \dots, e^X(T))$, gas consumption $g^X = (g^X(1), \dots, g^X(T))$, and amount of heat $q^X = (q^X(1), \dots, q^X(T))$ represent the energy flows; the X kinds of T -dimensional vectors $z^X = (z^X(1), \dots, z^X(T))$ of binary 0–1 decision variables represent the on-off status of each device in each term. The superscript X represents the index of each component in the PEFC-CGS. This MILP problem frames 1728 variables (28 kinds of linear variables \times 48 terms + 8 kinds binary variables \times 48 terms) and 2021 constraints. In order to check inner states and energy flows, we add some variables for the problem, which is composed the requisite minimum number of variables, therefore the problem has some redundant variables. As shown in Figure 4, the PEFC-CGS consists of four main parts: the polymer electrolyte membrane fuel cell (PEFC) unit, the thermal storage tank with a capacity V^{HWT} of 200 liters, in which perfect mixing hot water inside, the auxiliary boiler with an 83% conversion

efficiency η^B (based on lower heating value of the fuel: LHV), and the electric heater (H) with a 95% conversion efficiency η^H to hot water. Electricity demand is supplied from the grid and the PEFC unit. Because reverse flow of electricity from a CGS to the grid is not allowed in Japan, the surplus electricity produced by the CGS is supplied to the electric heater to prevent this. The rated hot water output of the PEFC unit is 1.0 kW (100% load). The DHW demand is supplied from the auxiliary boiler, in case the PEFC unit and the thermal storage tank cannot meet demand.

Figure 4. PEFC-CGS.



The relationship between the output of the PEFC unit and gas consumption is identified as a piecewise-linear function based on the measured data, as shown in Figure 5. Table 2 shows the partial load efficiency of the PEFC unit; the rated efficiency is the catalog value [20]. The rated electricity output is 0.7 kW. At the rated load, the total system efficiency is $50.0 + 35.0 = 85.0\%$, and the heat-to-power ratio at the rated output is $50.0/35.0 = 1.43$. The minimum electricity output is 0.25 kW (35.7% load), and the heat-to-power ratio of the output is $30.0/30.0 = 1.0$.

Table 2. Partial load performance of PEFC unit.

Load factor %	35.7	71.4	100
Electricity power output kW	0.25	0.50	0.70
Electricity power efficiency (LHV) %	30.0	34.0	35.0
Thermal efficiency (LHV) %	30.0	45.0	50.0

Figure 5. Partial load characteristics of PEFC unit.

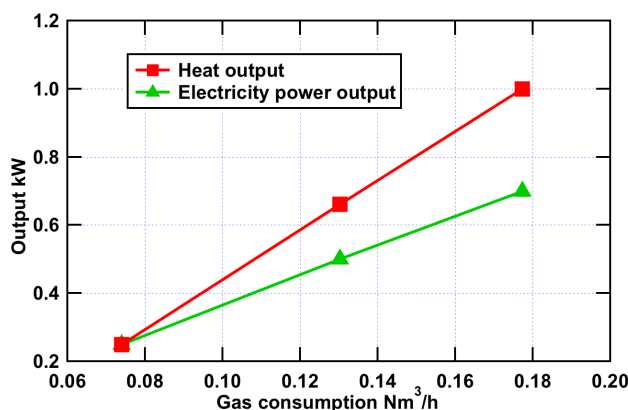


Table 3 shows the specifications of devices except the PEFC unit. The gas consumption of the PEFC unit g^{FC} has the following constraints:

$$\underline{G}_{rate1}^{FC} z_{rate1}^{FC}(t) \leq g_{rate1}^{FC}(t) \leq \overline{G}_{rate1}^{FC} z_{rate1}^{FC}(t) \tag{14}$$

$$\underline{G}_{rate2}^{FC} z_{rate2}^{FC}(t) \leq g_{rate2}^{FC}(t) \leq \overline{G}_{rate2}^{FC} z_{rate2}^{FC}(t) \tag{15}$$

$$g^{FC}(t) = g_{rate1}^{FC}(t) + g_{rate2}^{FC}(t) \tag{16}$$

$$z^{FC}(t) = z_{rate1}^{FC}(t) + z_{rate2}^{FC}(t) \tag{17}$$

$$z_{rate1}^{FC}(t) = \begin{cases} 1: \text{electricity output of the PEFC unit is between 0.25 and 0.50 kW in } t \text{ term} \\ 0: \text{otherwise} \end{cases} \tag{18}$$

$$z_{rate2}^{FC}(t) = \begin{cases} 1: \text{electricity output of the PEFC unit is between 0.50 and 0.70 kW in } t \text{ term} \\ 0: \text{otherwise} \end{cases} \tag{19}$$

where z^{FC} represents start-up status of the PEFC-CGS, \underline{G}^{FC} and \overline{G}^{FC} represent the lower and upper limit of the gas consumption in each rate. Therefore, electricity output e^{FC} and hot water output q^{FC} are given by:

$$e^{FC}(t) = \alpha_{rate1}^e g_{rate1}^{FC}(t) + \beta_{rate1}^e z_{rate1}^{FC}(t) + \alpha_{rate2}^e g_{rate2}^{FC}(t) + \beta_{rate2}^e z_{rate2}^{FC}(t) \tag{20}$$

$$q^{FC}(t) = \alpha_{rate1}^q g_{rate1}^{FC}(t) + \beta_{rate1}^q z_{rate1}^{FC}(t) + \alpha_{rate2}^q g_{rate2}^{FC}(t) + \beta_{rate2}^q z_{rate2}^{FC}(t) \tag{21}$$

where α^e , β^e , α^q , and β^q represent the slope and intercept of electricity and hot water output in each rate, respectively.

Table 3. PEFC-CGS specifications.

Specification		Value
Auxiliary boiler efficiency %	η^B	83.0
Controller electricity consumption W	E^C	10.0
Coefficient of thermal loss %/h	η^{HWT}	1.3
Electric heater efficiency %	η^H	95.0
Electricity consumption of pump for cyclic water W	E^{P1}	10.0
Electricity consumption of pump for heat circulation W	E^{P2}	50.0
Electricity consumption of pump for hot water W	E^{P3}	70.0
Electricity consumption of radiator fan W	E^R	15.0
Electricity consumption of start-up in first term Wh/30min	$E_{up,1}^{FC}$	300.0
Electricity consumption of start-up in second term Wh/30min	$E_{up,2}^{FC}$	200.0
Gas consumption of start-up in first term Nm ³ /30min	$G_{up,1}^{FC}$	0.016
Gas consumption of start-up in second term Nm ³ /30min	$G_{up,2}^{FC}$	0.024
Hot water outlet temperature from the PEFC unit °C	θ^{FC}	60.0
Minimum ratio of thermal storage tank %		10.0
Thermal storage tank capacity L	V^{HWT}	200.0

Hot water is stored by the thermal storage tank:

$$\begin{cases} q^{\text{HWT}}(1) = \left(1 - \frac{\eta^{\text{HWT}}}{100} \delta t\right) q^{\text{HWT}}(T) + q_{\text{in}}^{\text{HWT}}(T) - q_{\text{out}}^{\text{HWT}}(T) & \text{for } t = 1 \\ q^{\text{HWT}}(t) = \left(1 - \frac{\eta^{\text{HWT}}}{100} \delta t\right) q^{\text{HWT}}(t-1) + q_{\text{in}}^{\text{HWT}}(t-1) - q_{\text{out}}^{\text{HWT}}(t-1) & \text{for otherwise} \end{cases} \quad (22)$$

where q^{HWT} represents the amount of heat in the thermal storage tank, $q_{\text{out}}^{\text{HWT}}$ represents the amount of heat supplied for demand from the thermal storage tank, $q_{\text{in}}^{\text{HWT}}$ represents the amount of heat supplied for the thermal storage. The maximum amount of heat of the thermal storage tank is given by:

$$q^{\text{HWT}}(t) \leq \rho V^{\text{HWT}} c \{ \theta^{\text{FC}} - \theta^{\text{W}}(t) \} \quad (23)$$

where ρ represents water density, c represents specific heat of water, θ^{FC} represents hot water outlet temperature from the PEFC unit. θ^{W} represents feed-water temperature, and is measured data in each term. In case of oversupplying hot water, the radiator fan promote heat loss q^{R} . The status of the radiator fan, z^{R} , has the following constraints:

$$\frac{q^{\text{R}}(t)}{M} \leq z^{\text{R}}(t) \leq \frac{q^{\text{HWT}}(t)}{\rho V^{\text{HWT}} c \{ \theta^{\text{FC}} - \theta^{\text{W}}(t) \}} \quad (24)$$

where M represents a large number, which is so-called ‘‘Big-M’’. Therefore, energy balance around the thermal storage tank is given by:

$$q^{\text{FC}}(t) + q^{\text{H}}(t) = q_{\text{in}}^{\text{HWT}}(t) + q^{\text{R}}(t) \quad (25)$$

$$q^{\text{H}}(t) = \frac{\eta^{\text{H}}}{100} e^{\text{H}}(t) \quad (26)$$

where q^{H} and e^{H} represent the amount of heat and electricity consumption of the electric heater, respectively. The amount of heat q^{B} , which is supplied from the auxiliary boiler to demand, is given by:

$$q^{\text{B}}(t) = \frac{\eta^{\text{B}}}{100} H g^{\text{B}}(t) \quad (27)$$

where H represents the LHV of the fuel, and g^{B} represents the gas consumption of the auxiliary boiler. Therefore, hot water demand Q^{dem} in each term is satisfied with following equation:

$$Q^{\text{dem}}(t) = q_{\text{out}}^{\text{HWT}}(t) + q^{\text{B}}(t) \quad (28)$$

When starting up, the PEFC-CGS has the following three warming-up requirements: 60 minutes, 0.5 kWh of electricity, and 0.04 Nm³ of gas consumption. The start-up formulations are shown below:

$$z^{\text{FC}}(t) - z^{\text{FC}}(t-1) \leq z_{\text{up},2}^{\text{FC}}(t-1) \quad (29)$$

$$z_{\text{up},1}^{\text{FC}}(t-1) = z_{\text{up},2}^{\text{FC}}(t) \quad (30)$$

where $z_{\text{up},1}^{\text{FC}}$ is the first start-up term, and $z_{\text{up},2}^{\text{FC}}$ is the second start-up term. Gas consumption for start-up, $g_{\text{up}}^{\text{FC}}$, and electricity consumption for start-up, $e_{\text{up}}^{\text{FC}}$, are defined by:

$$g_{up}^{FC}(t) = G_{up,i}^{FC} z_{up,i}^{FC}(t) \tag{31}$$

$$e_{up}^{FC}(t) = E_{up,i}^{FC} z_{up,i}^{FC}(t) \tag{32}$$

where $i = \{1,2\}$ represents the start-up term.

The electricity demand E^{dem} for each term as well as gas consumption balance are satisfied with following equation:

$$e^{buy}(t) + (e^{FC}(t) - e^H(t)) = E^{dem}(t) + e_{up}^{FC}(t) + e^{AUXS}(t) \tag{33}$$

$$g^{buy}(t) = g^{FC}(t) + g^B(t) + g_{up}^{FC}(t) \tag{34}$$

where e^{AUXS} represents the electricity consumption of the auxiliary machines, in particular:

$$e^{AUXS}(t) = (E^C + E^{P1} z^{FC}(t) + E^{P2} z^B(t) + E^{P3} z^{HW}(t) + E^R z^R(t)) \delta t \tag{35}$$

$$\frac{q^B(t)}{M} \leq z^B \tag{36}$$

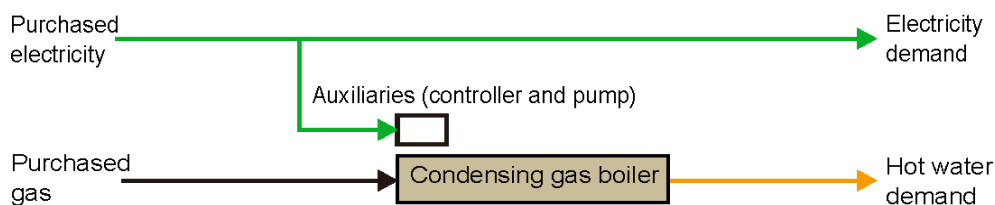
$$z^{HW}(t) = \begin{cases} 1: \text{there is DHW demand in } t \text{ term} \\ 0: \text{otherwise} \end{cases} \tag{37}$$

where z^B represents the on-off status of the auxiliary boiler.

4.3. Reference System (R-S)

Figure 6 shows the reference system: a condensing gas boiler, which has a 92% conversion efficiency (LHV), with electricity from the grid. DHW demand is supplied from the boiler on a just-in-time basis. Electricity demand is supplied from the grid only. Electricity consumption for the controller is 5 W, and for pump, 70 W. The best operation can be easily identified because the R-S has no energy buffers.

Figure 6. R-S.



5. Numerical Results

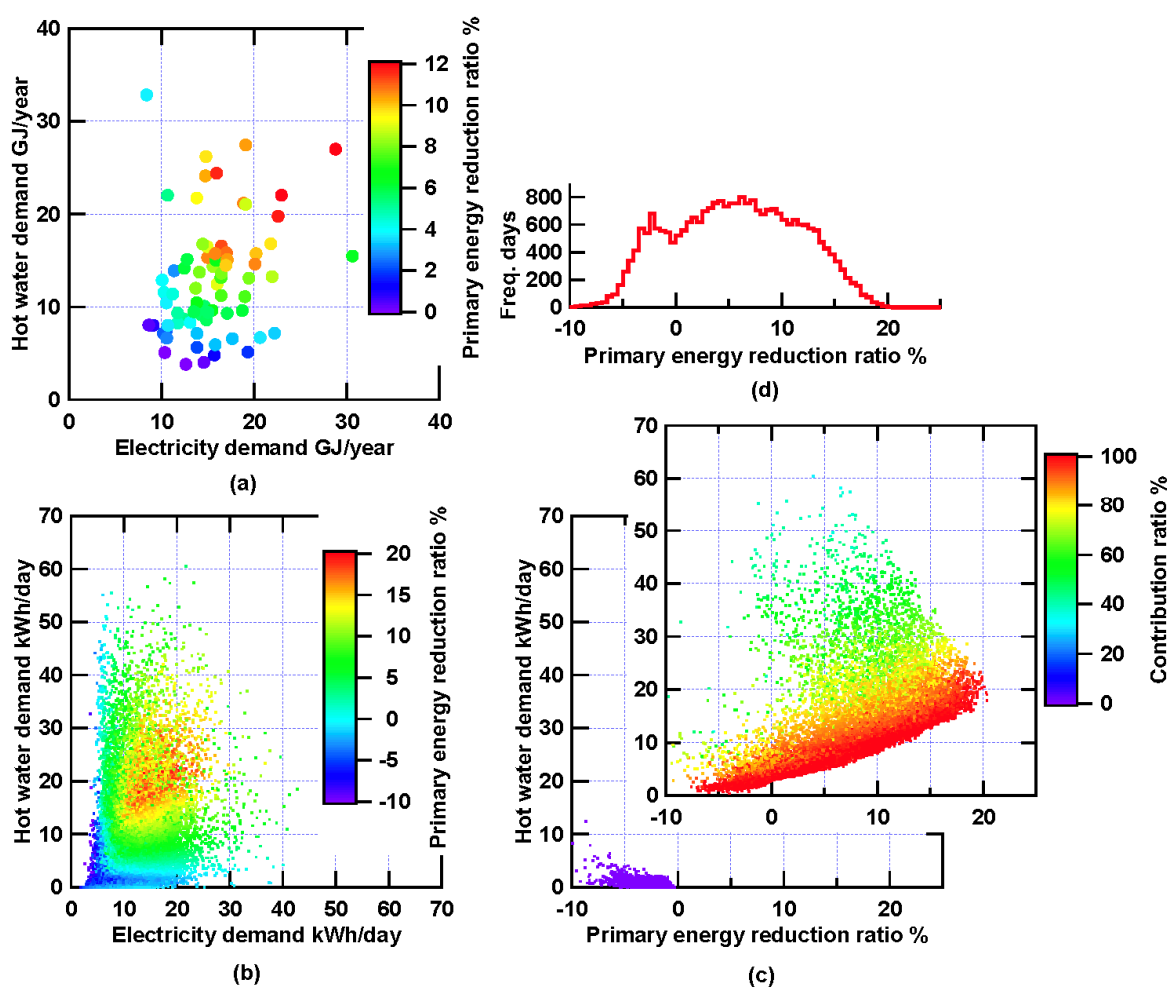
5.1. Optimal Operation

An index, φ , representing the primary energy reduction ratio is introduced:

$$\varphi = \frac{J_{RS} - J_{FC}}{J_{RS}} \times 100 \tag{38}$$

where J_{RS} represents the primary energy consumption of the R-S. Figure 7 shows the distribution of the daily primary energy reduction ratio. The average of all 26307 days of the primary energy reduction ratio is 5.64%, and the annual primary energy reduction ratios of each household, which are shown in Figure 7(a), are between -0.33% and 12.08% . It was found that an increase in annual demand is associated with a reduction in annual primary energy use.

Figure 7. Distribution of primary energy reduction ratio in optimal operation. (a) annual; (b) daily; (c) DHW demand vs. daily primary reduction ratio with contribution ratio; (d) frequency of primary energy reduction ratio.



The daily primary energy reduction ratios, which are shown in Figure 7(b), are between -11.71% and 20.34% . Reddish points, which indicate good performance with the PEFC-CGS, are scattered around an electricity demand of 15 kWh/day and a DHW demand of 20 kWh/day. It is found that, from the viewpoint of daily demand, the PEFC-CGS performs well around the rated output through a day; the electricity output is 16.8 kWh/day ($= 0.7 \text{ kW} \times 24 \text{ hour}$), and the thermal output is 24 kWh/day ($= 1.0 \text{ kW} \times 24 \text{ hour}$). From Figure 7(c), it can be seen that there is a peak in the primary energy reduction ratio around a DHW demand of 20 kWh/day. One of the dominant factors, the negative primary energy reduction ratio, is the case of hot water supplied by the auxiliary boiler on the PEFC-CGS. This is because the efficiency of the auxiliary boiler of the PEFC-CGS is inferior to that

of the condensing gas boiler of the R-S. There are two possible cases: the PEFC-CGS operation is inefficient because of too low DHW demand in the case of under the lower part load capacity of the PEFC-CGS, or too high DHW demand when shortage of heat supply was covered by the auxiliary boiler.

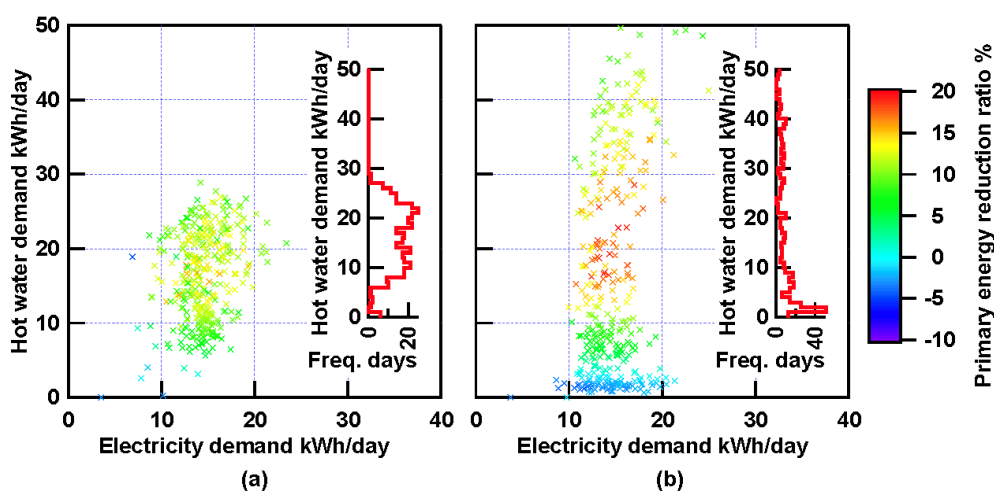
Here we introduce the contribution ratio, γ , of the PEFC unit:

$$\gamma = \sum_{t=1}^T \left(\frac{q^{\text{FC}}(t)}{q^{\text{FC}}(t) + q^{\text{B}}(t) + q^{\text{H}}(t)} \right) \times 100 \quad (39)$$

Whenever the PEFC unit is not used throughout a day, the contribution ratio is 0%, which is shown with purple points in Figure 7c. In these cases, the characteristics of the PEFC-CGS don't match the demand, because of lower DHW demand for the operations of the PEFC-CGS over an entire day. When using the PEFC unit at a low level of daily DHW demand, the primary energy reduction ratios are distributed throughout the negative values in Figures 7(c,d).

Due to space limitations, when comparing the differences among houses, we pick two houses, both of whom have the same level of annual demand. Table 4 shows the details of the household's characteristics. Figure 8 shows the scattered points of daily demand with the primary reduction ratios.

Figure 8. Daily primary energy reduction ratio. (a) House A; (b) House B.



The distribution of daily demand varies even though the families have the same level of annual demand. The DHW demand of House B is normally around 2 kWh/day; on the other hand, the maximum DHW demand is up to around 50 kWh/day.

Table 4. Characteristics of the two houses.

	(a) House A	(b) House B
Annual electricity demand GJ/year	18.83	19.06
Annual DHW demand GJ/year	21.20	21.06
Residential type	Detached house	Apartment
Age of householder	40's	50's
Number of occupants	4	4
Annual primary energy reduction ratio %	10.32	7.73
Range of daily primary energy reduction ratio %	-4.50~16.03	-4.35~19.60

Furthermore, it shows a difference in the primary energy reduction ratio even when daily demand is the same, House B has more reddish points than House A around an electricity demand of 15 kWh/day and DHW demand of 20 kWh/day. It seems effected by demand patterns.

5.2. Extraction of Demand Patterns

Six sets of groups of demand were defined by the heat-to-power ratio and the daily DHW demand. Group-A does not show a significant difference because this proposed method, fitted GMDs for demand patterns, is difficult to adapt to low demand situations, including 0 kWh/day. This is a disadvantage of this method; in short, it is necessary to exclude days which have a low level of demand, including 0 kWh/day, before the data are used for statistical processing. Hence Figures 9 to 13 show the demand patterns clustered in 16 groups for Groups B to F. The green bar charts represent the average electricity demand of each term in each cluster; the red cityscapes represent the average DHW demand, the black and red dotted lines represent the electricity and DHW demand \pm standard deviation on average of each term. The rightmost pictures in Figures 9 to 13 are dendrograms which represent hierarchical structures. If trying to decrease the number of clusters, concatenate the adjacent clusters. It is confirmed that the basic demand patterns are extracted by the hierarchical clustering with the generalized KL divergence, and reveal the demand pattern's structures. Figure 14 shows cluster histograms labeled with a monthly perspective; the vertical axis label shows "Group name—Cluster number". For example, in Figure 14(a) the bar labeled "C-5" is the modal class, "C-5" means this bar belongs to Cluster 5 in Group C. Summer days, which are shown with bluish bars, are mostly in Group C. In House B, the spring days are found many in Group A.

In House B, the day marked 19.60% of the highest primary energy reduction ratio is grouped in "D-11", the day marked 18.78% of the second highest primary energy reduction ratio is grouped in "D-1", and the next is grouped in "D-5". It is confirmed that there are clusters which are distributed among the higher primary energy reduction ratios in Figure 11, "D-11", "D-1", and "D-5". We compare these clusters to "D-2", which is the modal class of House A in Group D, "D-2" has no peak in the morning. Comparing all clusters in Figure 11 from the same viewpoint, the primary energy reduction ratios of "D-3", "D-9", "D-10", "D-13", and "D-14" are distributed over a wide range, and these patterns do not have large peaks in the morning. Similarly, demand patterns having several gentle slopes perform well with the PEFC-CGS, as, for example, "E-1", "E-11", "E-12", "E-15", and "E-16" in Figure 12. Hence, it is found that demand patterns having several gentle slopes shows better primary energy reduction ratios.

Figure 9. Clusters in Group B. (a) primary energy reduction ratio; (b) demand patterns; (c) dendrogram.

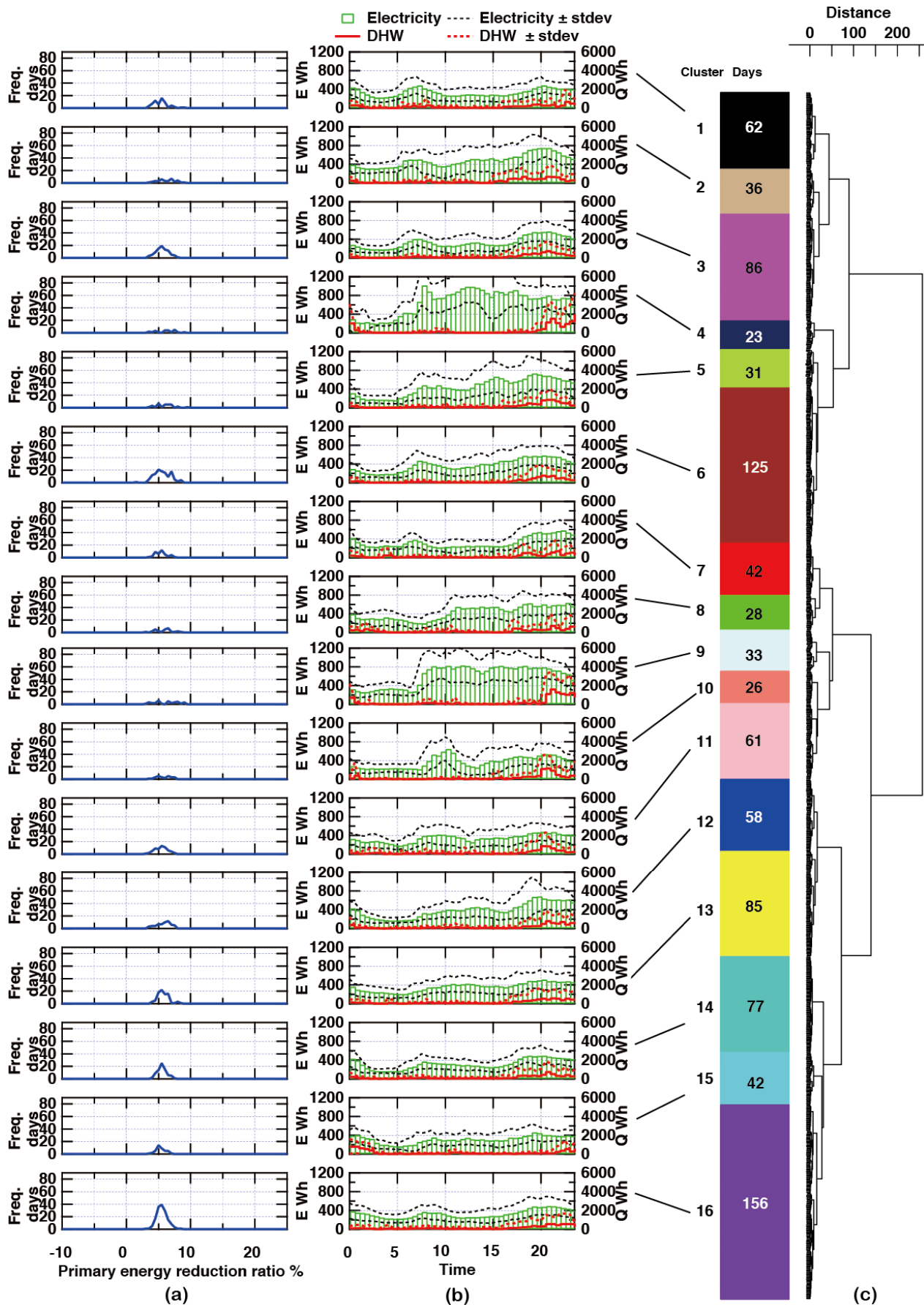


Figure 10. Clusters in Group C. (a) primary energy reduction ratio; (b) demand patterns; (c) dendrogram.

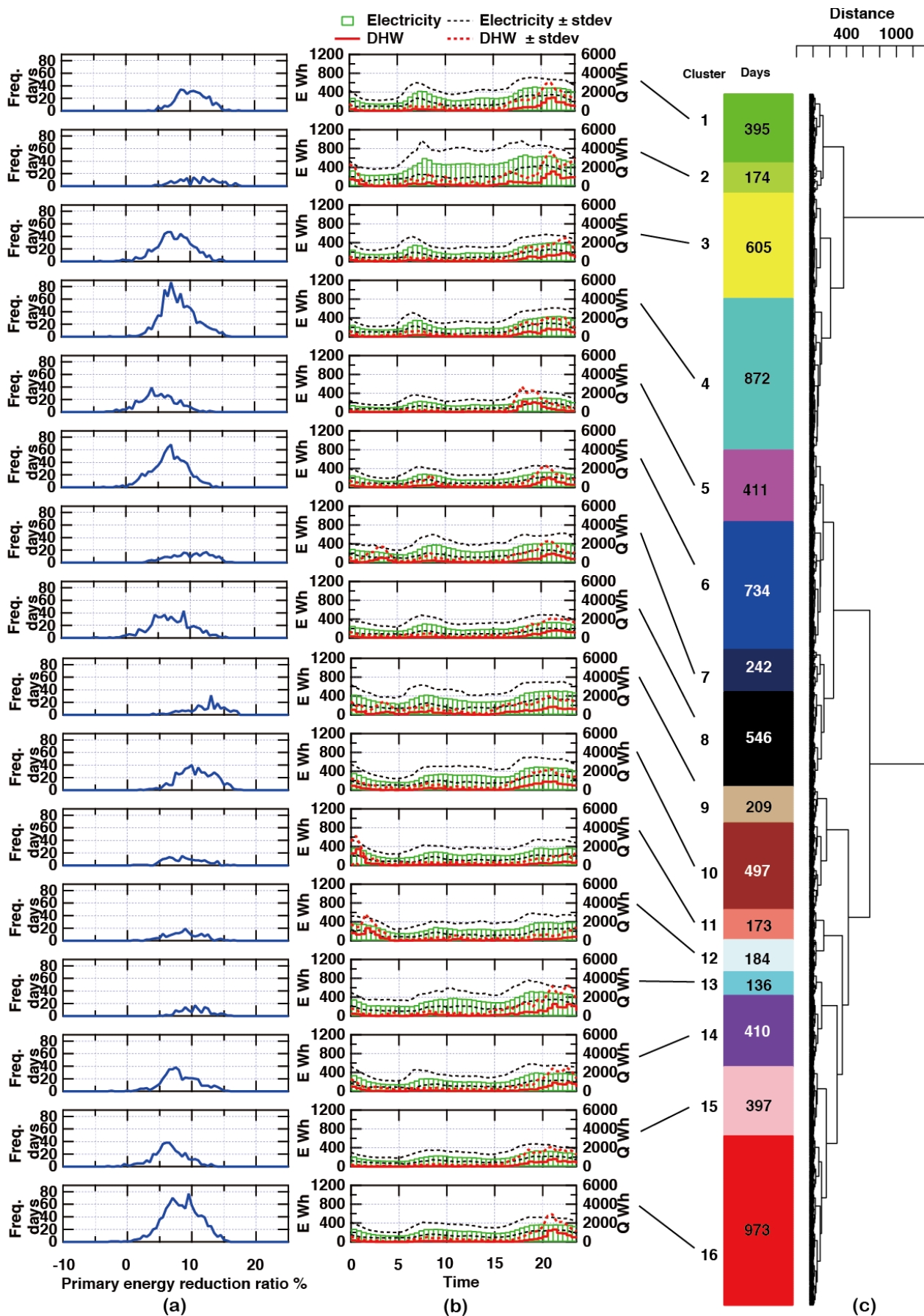


Figure 11. Clusters in Group D. (a) primary energy reduction ratio; (b) demand patterns; (c) dendrogram.

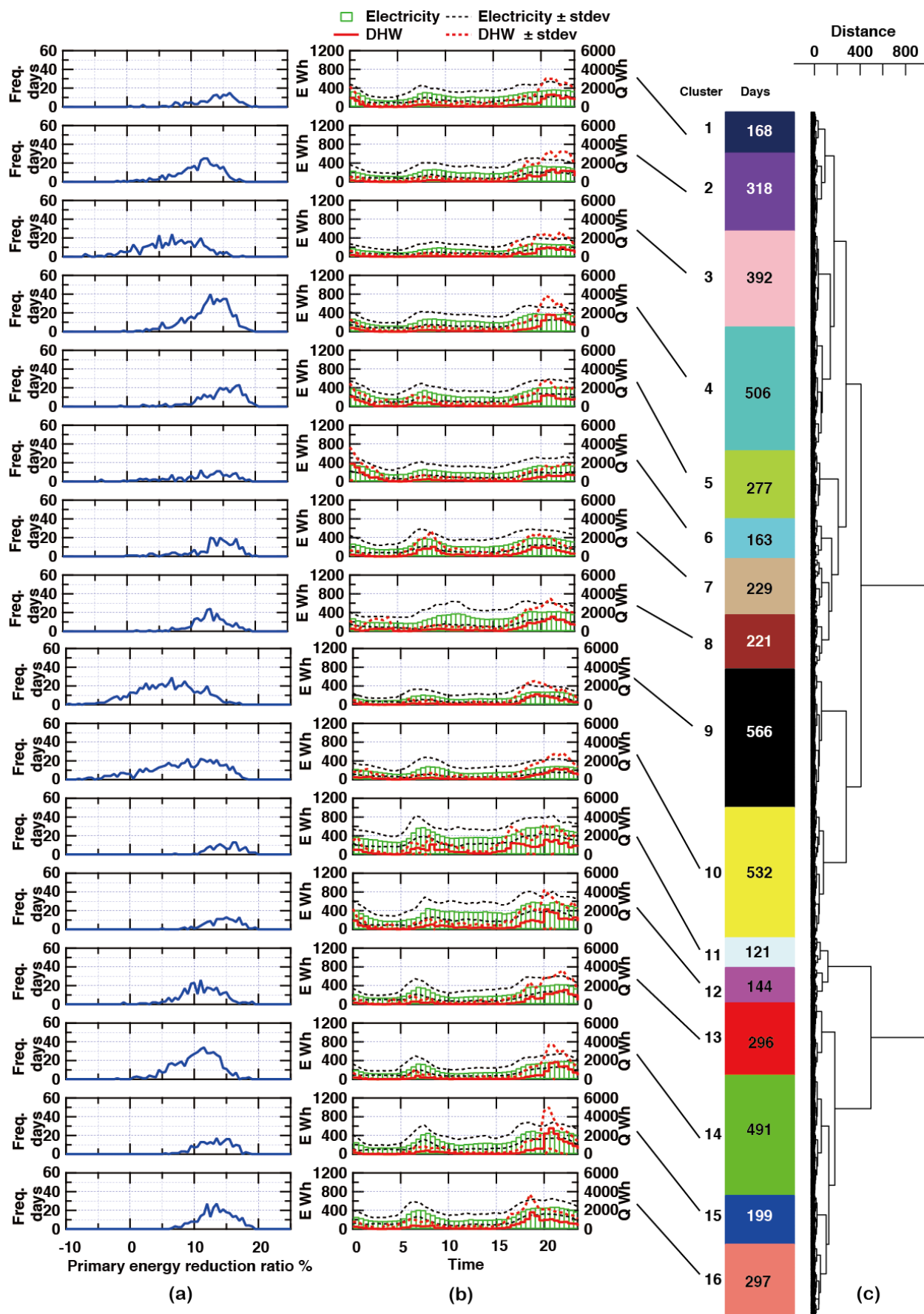


Figure 12. Clusters in Group E. (a) primary energy reduction ratio; (b) demand patterns; (c) dendrogram.

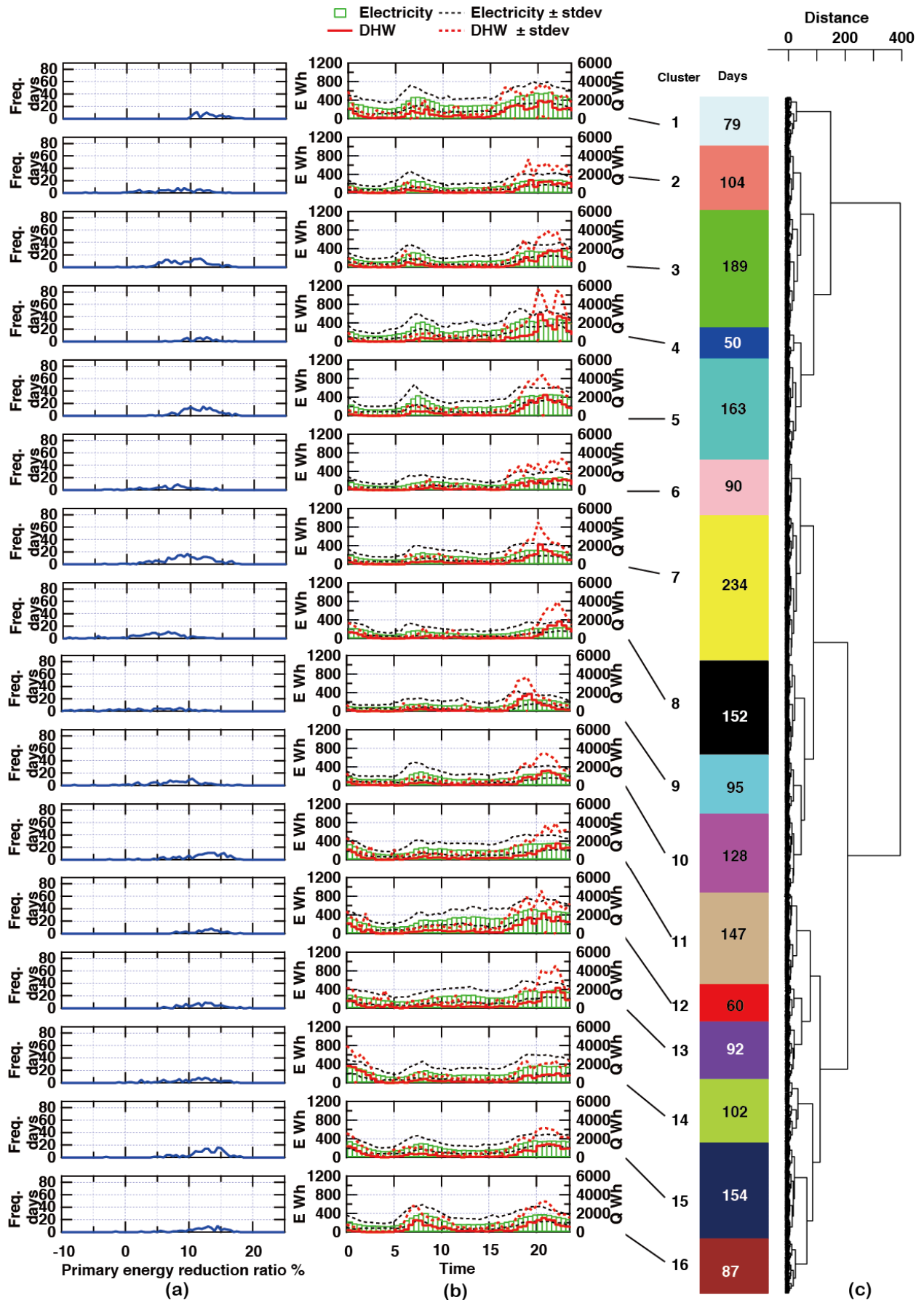


Figure 13. Clusters in Group F. (a) primary energy reduction ratio; (b) demand patterns; (c) dendrogram.

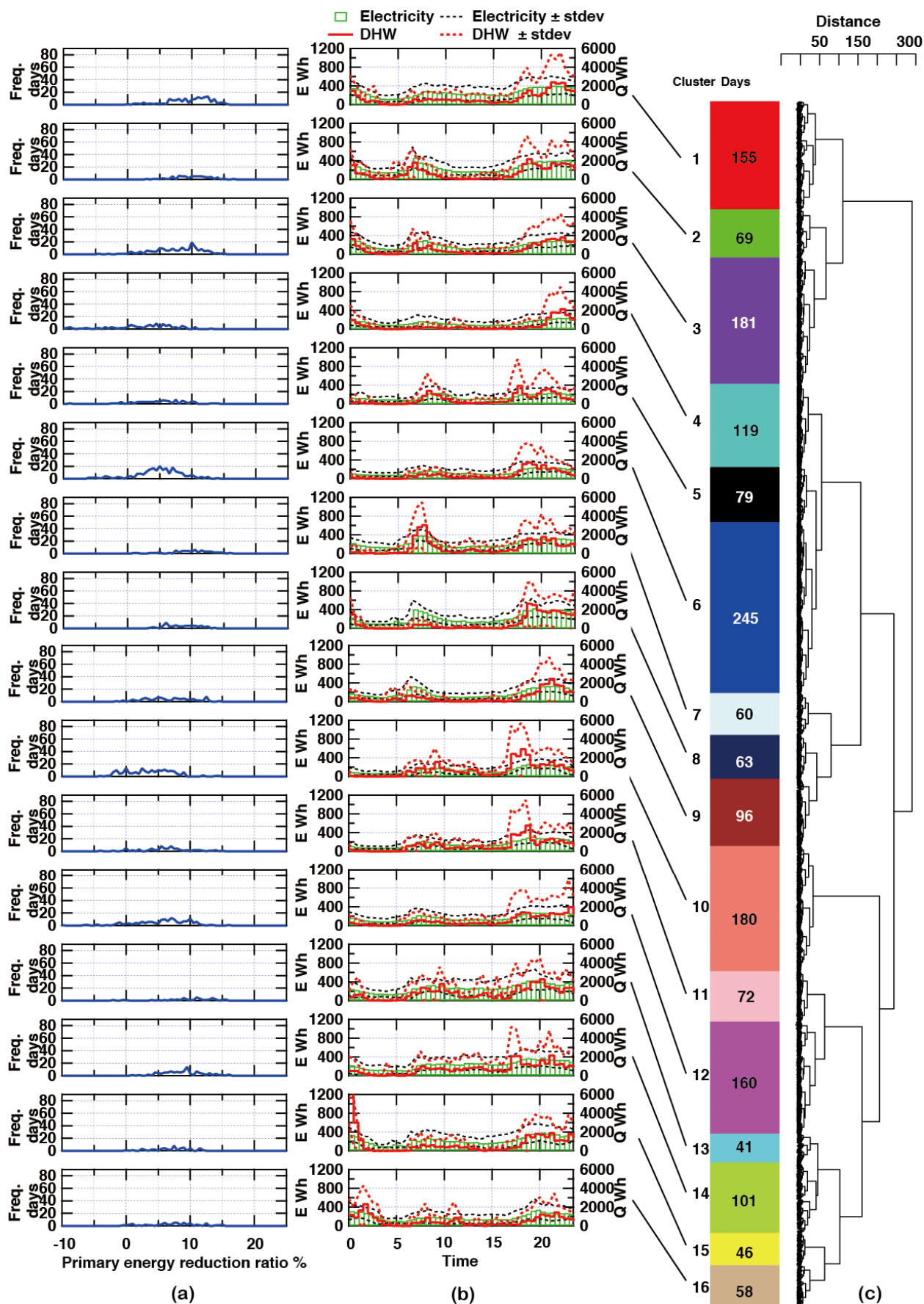
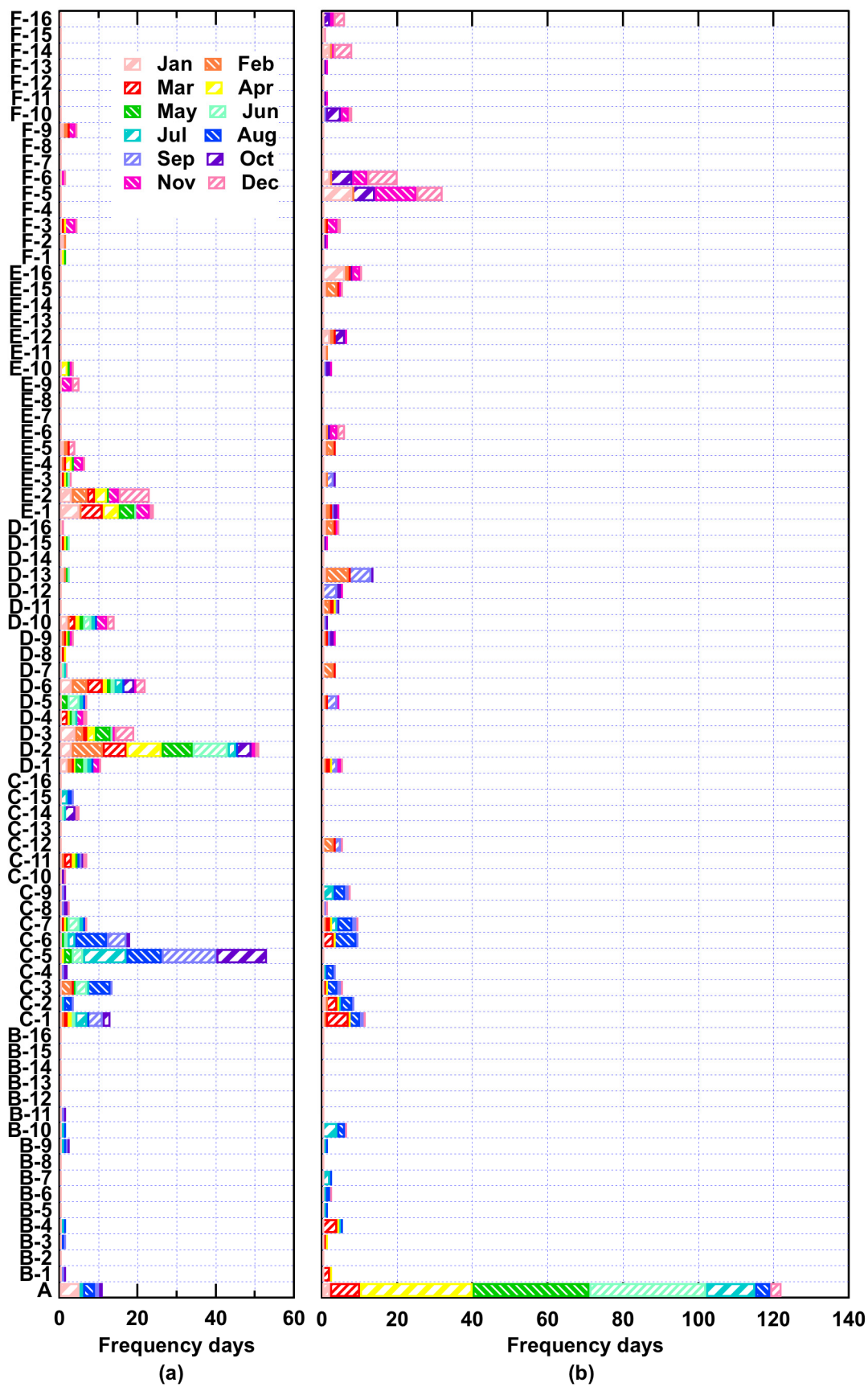


Figure 14. Cluster histograms labeled from a monthly perspective. (a) House A; (b) House B.



In Figure 14, House A has many similar demand patterns, which do not have a large peak in the morning, without little effect of the seasons, for example “C-1”, “C-3”, “C-5”, “C-6”, “D-2”, and “D-3”. On the other hand, demand patterns of House B are scattered on many clusters, which mean having many life patterns. Thus, it is found that the demand characteristics for each house have different features; one house shows a weak association between DHW demand and seasons, and the other shows a strong association between them.

The result of this paper revealed that the level of demand and the heat-to-power ratio were the most important for screening the matching between the demand profiles and the energy saving potential of the PEFC-CGS, while demand patterns took second place. In the future, householders will estimate their demand characteristics with access to an increasing number of residential demand patterns measured using the Home Energy Management System and such. Such demand patterns are capable of denoting a relationship to demographic data, such as the number of people in the household, their life patterns, age composition and so on. In that case, they will get to be able to select an energy supply system which matches the characteristics of the system and the characteristics of their demands.

6. Conclusions

Time-series demand data are categorized by means of a hierarchical clustering method using a statistical pseudo-distance. The statistical pseudo-distance is represented by the generalized KL divergence of two GMDs fitted to the time-series demand data of non-HVAC electricity and DHW demand from 26,307 days of data, measured in Japan. We formulated an analytical framework of the characteristics of the energy systems, and of the characteristics of the demand profiles. The following main results were obtained:

1. Basic demand patterns are extracted from 72 households 26,307 days of data by the proposed method.
2. The factors which are at least associated with the primary energy reduction ratio of the PEFC-CGS, are heat-to-power ratio, the amount of daily demand, and the demand patterns.
3. By installing the PEFC-CGS, the annual primary energy reduction ratio is about 12% maximum, and an increase in annual demand is associated with a reduction in annual primary energy use.
4. By installing the PEFC-CGS, daily primary energy reduction ratio is about 20% maximum near a DHW demand of 20 kWh/day, which is operated with the rated power output throughout a day.
5. Daily reduction ratios are different between one day and another even if the amount of daily demand is the same.
6. Demand patterns having several gentle slopes show better primary energy reduction ratios.
7. Demand characteristics in different houses have different features. One house shows a weak association between DHW demand and seasons; another shows a strong association between them.

Acknowledgments

The authors acknowledge Haoyang Shen and Hideitsu Hino of the Murata Laboratory of Waseda University for technical suggestions about implementation using the R language. Part of this work is supported by a Strategic Research Foundation Grant-aided Project for Private Universities grant from MEXT (2010). The authors would like to acknowledge the support of the “Distributed Autonomous Urban Energy Systems for Mitigating Environmental Impact” project of Osaka University. This research was conducted under Optimal Planning of Energy Supply Systems for Various Buildings, 09P05 at RISE, Waseda University.

References

1. *EDMC Handbook of Energy & Economic Statistics in JAPAN 2012*; The Institute of Energy Economics: Tokyo, Japan, 2012; pp. 88–109.
2. Nakagami, H.; Murakoshi, C.; Iwafune, Y. International Comparison of Household Energy Consumption and Its Indicator. In *Proceedings of the 2008 ACEEE Summer Study on Energy Efficiency in Buildings*, Pacific Grove, CA, USA, 17–22 August 2008; pp. 214–224.
3. Yokoyama, R.; Ito, K. Optimal operational planning of cogeneration systems with thermal storage by the decomposition method. *J. Energy Resour. Technol.* **1995**, *117*, 337–342.
4. Wakui, T.; Yokoyama, R.; Shimizu, K. Suitable operational strategy for power interchange operation using multiple residential SOFC (solid oxide fuel cell) cogeneration systems. *Energy* **2010**, *35*, 740–750.
5. Hashimoto, K.; Takahashi, T.; Yoshiha, T.; Saikawa, M.; Hamamatsu, T. *Evaluation of Energy Saving and Environment Potential about New Domestic Energy Systems—Comparison of Hot Water Supplying and Air-Conditioning Electric Heat Pumps, and of PEFC Co-Generation, with Consideration to Daily and Yearly Estimated Demand Curve*; Central Research Institute of Electric Power Industry: Kanagawa, Japan, 2001.
6. Arndt, U.; Beausoleil-morrison, I.; Brouwer, J.; Viktor, D.; Ferguson, A.; Griffith, B.; Kelly, N.; Klobut, K.; Knight, I.; Lie, B.; *et al.* *An Experimental and Simulation-Based Investigation of the Performance of Small-Scale Fuel Cell and Combustion-Based Cogeneration Devices Serving Residential Buildings*; Natural Resource Canada: Ontario, Canada, 2008.
7. Dorer, V.; Weber, A. Energy and CO₂ emissions performance assessment of residential micro-cogeneration systems with dynamic whole-building simulation programs. *Energy Convers. Manag.* **2009**, *50*, 648–657.
8. Yoshida, A.; Inagaki, K.; Amano, Y.; Ito, K.; Hashizume, T. Comparative evaluation of residential energy systems to reduce CO₂ emissions. In *Proceedings of World Engineers Convention 2011*, Geneva, Switzerland, 4–9 September 2011; pp. 2–9.
9. Bishop, C.M. *Pattern Recognition and Machine Learning*; Springer: New York, NY, USA, 2006.
10. Hershey, R.J.; Olsen, A.P. Approximating the Kullback Leibler divergence between Gaussian mixture models. In *Proceedings of the International Conference on Acoustics, Speech, and Signal Processing 2007*, Glasgow, Scotland, 24–28 June 2007; pp. 317–320.

11. Shen, H.; Hino, H.; Murata, N.; Wakao, S. Extraction of basic patterns of household energy consumption. In *Proceedings of the Tenth International Conference on Machine Learning and Applications*; Honolulu, HI, USA, 18–21 December 2011; pp. 275–280.
12. Kosmelj, K.; Batagelj, V. Cross-sectional approach for clustering time varying data. *J. Classif.* **1990**, *7*, 99–109.
13. Liao, W.T. Clustering of time series data—a survey. *Pattern Recognit.* **2005**, *38*, 1857–1874.
14. Tsuji Laboratory. *Monitored Energy Data for Residential Houses in Kansai Region 1998–2005*; Osaka University, Osaka, Japan, 2007.
15. Banerjee, A.; Merugu, S.; Dhillon, I.S.; Ghosh, J. Clustering with Bregman divergences. *J. Mach. Learn. Res.* **2005**, *6*, 1705–1749.
16. Dempster, A.P.; Laird, N.M.; Rubin, D.B. Maximum likelihood from incomplete data via the EM algorithm. *J. R. Stat. Soc.* **1977**, *39*, 1–38.
17. Fraley, C.; Raftery, A.E. *MCLUST Version 3 for R: Normal Mixture Modeling and Model-Based Clustering*; Technical Report, University of Washington, Washington, WA, USA, 2006; pp. 1–57.
18. Schwarz, G. Estimating the dimension of a model. *Annu. Stat.* **1978**, *6*, 461–464.
19. Ward, H.J. Hierarchical grouping to optimize an objective function. *J. Am. Stat. Assoc.* **1963**, *58*, 236–244.
20. Toshiba Fuel Cell Power Systems Co. Available online: <http://www.toshiba.co.jp/product/fc/products/pdf/catalog6.pdf> (accessed on 1 November 2012).
21. Fourer, R.; Gay, M.D.; Kernighan, W.B. *AMPL: A Modeling Language for Mathematical Programming*, 2nd ed.; Thomson/Brooks/Cole Publishing Company: Pacific Grove, CA, USA, 2003.
22. IBM ILOG CPLEX Optimizer. Available online: <http://www-01.ibm.com/software/integration/optimization/cplex-optimizer/> (accessed on 1 August 2012).
23. Osaka Gas Co. Available online: <http://www.osakagas.co.jp/kankyo/gas/03.html> (accessed on 1 August 2012).
24. Law Concerning the Rational Use of Energy in Japan. Available online: <http://law.e-gov.go.jp/htmldata/S54/S54F03801000074.html> (accessed on 1 August 2012).

© 2013 by the authors; licensee MDPI, Basel, Switzerland. This article is an open access article distributed under the terms and conditions of the Creative Commons Attribution license (<http://creativecommons.org/licenses/by/3.0/>).